An Improved UMEC Method for Modeling Arbitrary Magnetic Circuit in Real Time EMT Simulation

Dong Li
RTDS Technologies Inc.
Winnipeg, Canada
dong.li@ametek.com

Yi Zhang
RTDS Technologies Inc.
Winnipeg, Canada
yi.zhang@ametek.com

Ali B. Dehkordi
RTDS Technologies Inc.
Winnipeg, Canada
ali.dehkordi@ametek.com

Meysam Ahmadi
RTDS Technologies Inc.
Winnipeg, Canada
meysam.ahmadi@ametek.com

***Abstract*--Real-time EMT simulators are essential for analyzing dynamic behavior and testing hardware-in-the-loop systems in modern power grids. However, modeling magnetic circuits with arbitrary topologies and nonlinear behavior remains a challenge due to limitations in traditional methods like the Universal Magnetic Equivalent Circuit (UMEC) models. UMEC relies on fixed transformer configurations to exploit matrix sparsity and reduce computation cost. For arbitrary magnetic circuits, this sparsity advantage is lost, making real-time simulation impractical, particularly in systems with high penetration of power electronics that demand small time steps. This paper presents a novel method for modeling arbitrary magnetic circuits in EMT simulators by replacing variable reluctance with a fixed reluctance in parallel with a flux source. In the proposed method, both the admittance matrix and the current injection coefficients remain constant throughout the simulation. As a result, it enables efficient and scalable simulation of nonlinear magnetic circuits in real time, significantly expanding the applicability of EMT tools in electromagnetic system analysis.**

***Keywords*--Real-time simulation, Magnetic circuit, Nonlinear reluctance, Universal Magnetic Equivalent Circuit.**

I. Introduction

Modern power systems increasingly rely on complex magnetic components featuring custom core structures and unconventional winding arrangements [1][2]. Traditional modeling approaches in Electromagnetic Transients (EMT) simulators often depend on pre-defined and simplified magnetic circuit representations, which lack the flexibility to accurately capture diverse magnetic topologies. This limitation can lead to reduced accuracy in transient studies and increased effort in model development. The capability to simulate arbitrary magnetic circuits—regardless of geometry, material properties, or winding configuration—would significantly enhance the fidelity of EMT analyses and streamline the modeling process, enabling more robust and efficient design and validation of power system components.

EMT simulators such as EMTP-RV, PSCAD, and RTDS rely on the Dommel algorithm, which is highly efficient for solving large-scale electrical networks [3]. However, the Dommel algorithm does not provide direct support for multi-domain modeling in the way that state-space approaches (e.g., in Simulink or PLECS) do, because EMT components are formulated in terms of the terminal electrical behavior rather than explicit multi-domain physical equations. As a result, representing magnetic circuits, particularly those with arbitrary or complex topologies, remains challenging within the traditional EMT framework.

Scholars in [4][5] proposed a method for modeling multi-limb transformers based on their underlying magnetic circuit, known as the Universal Magnetic Equivalent Circuit (UMEC) model. Rather than representing each individual element of the magnetic circuit, the UMEC approach models the entire magnetic structure as a unified entity. This holistic magnetic model is then integrated into the electrical network as a companion circuit, allowing it to be solved within the EMT simulation framework using the Dommel algorithm.

The derivation of the UMEC model involves intensive matrix operations. When the magnetic circuit is linear, these computations remain constant and can be preprocessed before simulation begins. However, when core saturation is considered, the reluctance values become nonlinear and vary at each time step. This necessitates repeated matrix updates and factorization during simulation, significantly increasing computational burden and limiting the model's applicability in real-time EMT simulation. To address this, engineers in [6] proposed a reorganization of the UMEC method that leverages matrix sparsity. This enhancement enables the use of nonlinear UMEC models in real-time EMT environments by reducing per-step computational overhead.

While effective for standard transformer configurations, the UMEC model's reliance on fixed topologies limits its flexibility and scalability. Extending UMEC to support arbitrary magnetic circuits presents two key challenges:

1. First, it requires a systematic method to derive the core matrices (incidence matrix, turns matrix, and permeance matrix) from arbitrarily connected magnetic elements. These matrices are foundational to the UMEC formulation but are traditionally constructed manually for a certain topology.
2. Second, even after obtaining these matrices, the lack of inherent sparsity in arbitrary configurations poses a significant computational burden. The model must be improved to ensure that such models can be simulated in real time within EMT environments.

This study successfully addressed these challenges by:

1. Developing an automatic method for formation of UMEC matrices.
2. Developing a fixed-matrix UMEC algorithm that saturation is modeled based on flux injection.

This development enables arbitrary magnetic circuit simulation in real time EMT simulators. The method has been implemented and tested on RTDS NovaCor simulators. The users could use components such as electromagnetic converters (windings), linear reluctances and nonlinear reluctances to create arbitrary magnetic circuits and simulate in the EMT environment.

This paper is organized as follows: Section II reviews the conventional UMEC modeling procedure. Section III presents the proposed improved UMEC modeling framework, which enables arbitrary magnetic circuit simulation. Section IV benchmarks the proposed method against existing transformer models to validate accuracy and

979-8-3315-8138-1

performance. Section V demonstrates the application of the proposed tool by simulating a Multi-winding Coupled Inductor (MCI) for an interleaved dc-dc converter, highlighting its flexibility and real-time capability.

II. CONVENTIONAL UMEC APPROACH

Taking the single-phase two-winding transformer with loose magnetic coupling shown in Fig. 1 as an example, the conventional UMEC approach is explained in this session [7].

Fig. 1 shows the flux paths of this transformer. Fig. 2 shows the equivalent magnetic circuit, where branch fluxes are shown as ϕ_1-ϕ_5, branch MMFs are shown as θ_1-θ_5 and branch reluctance are shown as R_1-R_5. The magnetic circuit has three nodes, and any one of the nodes could be set to MMF reference point. In this demonstration we use node 3 as the reference point.

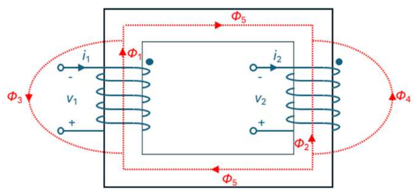

Fig. 1 Flux paths of a single-phase two-winding transformer.

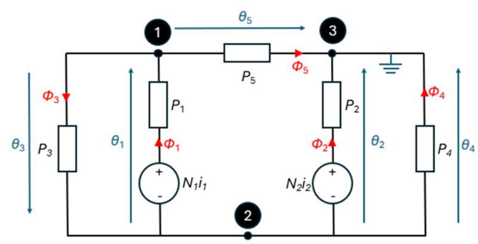

Fig. 2 Equivalent magnetic circuit, where branch fluxes are shown as ϕ_1-ϕ_5, branch MMFs are shown as θ_1-θ_5 and branch reluctances are shown as R_1-R_5.

For fluxes flow in/out node 1,

$$\Phi_1 - \Phi_3 - \Phi_5 = 0 \tag{1}$$

Similarly, for node 2,

$$-\Phi_1 - \Phi_2 + \Phi_3 - \Phi_4 = 0 \tag{2}$$

Combine (1) and (2),

$$\begin{bmatrix} 1 & 0 & -1 & 0 & -1 \\ -1 & -1 & 1 & -1 & 0 \end{bmatrix} \begin{bmatrix} \Phi_1 \\ \Phi_2 \\ \Phi_3 \\ \Phi_4 \\ \Phi_5 \end{bmatrix} = 0 \tag{3}$$

In matrix format,

$$\boldsymbol{A}^T \boldsymbol{\Phi} = 0 \tag{4}$$

where $\boldsymbol{A}^T = \begin{bmatrix} 1 & 0 & -1 & 0 & -1 \\ -1 & -1 & 1 & -1 & 0 \end{bmatrix}$ contains the information of branch connection, and is called incidence matrix.

For branch Magnetic Motive Forces (MMFs),

$$\begin{bmatrix} \theta_1 \\ \theta_2 \\ \theta_3 \\ \theta_4 \\ \theta_5 \end{bmatrix} = \begin{bmatrix} N1 & 0 & 0 & 0 & 0 \\ 0 & N2 & 0 & 0 & 0 \\ 0 & 0 & 0 & 0 & 0 \\ 0 & 0 & 0 & 0 & 0 \\ 0 & 0 & 0 & 0 & 0 \end{bmatrix} \begin{bmatrix} i_1 \\ i_2 \\ 0 \\ 0 \\ 0 \end{bmatrix} - \begin{bmatrix} R1 & 0 & 0 & 0 & 0 \\ 0 & R2 & 0 & 0 & 0 \\ 0 & 0 & R3 & 0 & 0 \\ 0 & 0 & 0 & R4 & 0 \\ 0 & 0 & 0 & 0 & R5 \end{bmatrix} \begin{bmatrix} \Phi_1 \\ \Phi_2 \\ \Phi_3 \\ \Phi_4 \\ \Phi_5 \end{bmatrix} \tag{5}$$

In matrix format,

$$\boldsymbol{\theta} = \boldsymbol{Ni} - \boldsymbol{R\Phi} \tag{6}$$

A branch MMF can be represented as difference of the two node MMFs. The relationship is shown below.

$$\begin{bmatrix} 1 & -1 \\ 0 & -1 \\ -1 & 1 \\ 0 & -1 \\ -1 & 0 \end{bmatrix} \begin{bmatrix} \theta_{node} \\ \theta_{node} \end{bmatrix} = \begin{bmatrix} \theta_1 \\ \theta_2 \\ \theta_3 \\ \theta_4 \\ \theta_5 \end{bmatrix} \tag{7}$$

In matrix format,

$$\boldsymbol{A}\,\boldsymbol{\theta}_{node} = \boldsymbol{\theta} \tag{8}$$

Equation (6) can be rewritten as,

$$\boldsymbol{\Phi} = \boldsymbol{P}(\boldsymbol{Ni} - \boldsymbol{\theta}) \tag{9}$$

where $\boldsymbol{P} = \boldsymbol{R}^{-1}$, is the permeance matrix.

Left multiplying $\boldsymbol{A}^T$ on both sides of equation (9).

$$\boldsymbol{A}^T\boldsymbol{\Phi} = \boldsymbol{A}^T\boldsymbol{PNi} - \boldsymbol{A}^T\boldsymbol{P\theta} \tag{10}$$

Apply (4) and (8) to (10).

$$0 = \boldsymbol{A}^T\boldsymbol{PNi} - \boldsymbol{A}^T\boldsymbol{PA}\,\boldsymbol{\theta}_{node} \tag{11}$$

$$\boldsymbol{\theta}_{node} = (\boldsymbol{A}^T\boldsymbol{PA})^{-1}\boldsymbol{A}^T\boldsymbol{PNi} \tag{12}$$

Left multiplying A and apply (8),

$$\boldsymbol{\theta} = \boldsymbol{A}(\boldsymbol{A}^T\boldsymbol{PA})^{-1}\boldsymbol{A}^T\boldsymbol{PNi} \tag{13}$$

Substituting (13) into (9),

$$\boldsymbol{\Phi} = \boldsymbol{MNi} \tag{14}$$

$$\text{where } \boldsymbol{M} = \boldsymbol{P} - \boldsymbol{PA}(\boldsymbol{A}^T\boldsymbol{PA})^{-1}\boldsymbol{A}^T\boldsymbol{P} \tag{15}$$

Notice that elements that are not related to winding branches in matrix $\boldsymbol{N}$ are zero as shown in (5). Thus, Equation (14) is partitioned into the set that contains the branches associated with windings,

$$\boldsymbol{\Phi}_{ss} = \boldsymbol{M}_{ss}\boldsymbol{N}_{ss}\boldsymbol{i}_{ss} \tag{16}$$

In this case, $\boldsymbol{\Phi}_{ss} = \begin{bmatrix} \Phi_1 \\ \Phi_2 \end{bmatrix}$, $\boldsymbol{M}_{ss} = \begin{bmatrix} M_{11} & M_{12} \\ M_{21} & M_{22} \end{bmatrix}$, $\boldsymbol{N}_{ss} = \begin{bmatrix} N_1 & 0 \\ 0 & N_2 \end{bmatrix}$, $\boldsymbol{i}_{ss} = \begin{bmatrix} i_1 \\ i_2 \end{bmatrix}$.

The winding terminal voltages,

$$\boldsymbol{v}(t) = \boldsymbol{N}_{ss}\frac{d\boldsymbol{\Phi}_{ss}(t)}{dt} = \boldsymbol{N}_{ss}\boldsymbol{M}_{ss}\boldsymbol{N}_{ss}\frac{d\boldsymbol{i}_{ss}(t)}{dt} \tag{17}$$

Discretize (17) with trapezoidal integration, the classic companion circuit representation can be obtained,

$$\boldsymbol{i}_{ss} = \boldsymbol{Gv} + \boldsymbol{i}_{his} \tag{18}$$

$$\text{where } \boldsymbol{G} = \frac{dt}{2}(\boldsymbol{N}_{ss}\boldsymbol{M}_{ss}\boldsymbol{N}_{ss})^{-1} \tag{19}$$

$$\text{and } \boldsymbol{i}_{his} = \frac{dt}{2}(\boldsymbol{N}_{ss}\boldsymbol{M}_{ss}\boldsymbol{N}_{ss})^{-1}\boldsymbol{v}(t-dt) + \boldsymbol{i}_{ss}(t-dt) \tag{20}$$

Fig. 3 shows how reluctance changes when the core is saturated. The slope of each dashed line represents reluctance value under each operating point. If reluctance nonlinearity is considered, permeance matrix $\boldsymbol{P}$ in (9) should be updated in each time step, and calculation in (15) and (19) need to be repeated in every time step, which significantly increases computation burden and limits its usage in real time simulation.

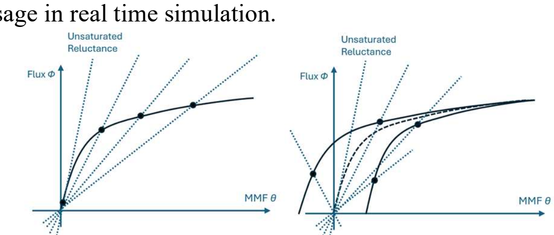

Fig. 3 Reluctance changes when saturated, (a) without hysteresis (b) with hysteresis.

III. PROPOSED APPROACHES

A. Matrix Formation for Arbitrary Magnetic Circuit

As introduced in session II, as long as the system matrices, including incidence matrix $\boldsymbol{A}$, turns matrix $\boldsymbol{N}$, and permeance matrix $\boldsymbol{P}$, are available, the companion circuit of the magnetic circuit can be derived. To achieve arbitrary magnetic circuit simulation, individual magnetic circuit components like winding, reluctance and nonlinear reluctance are made available to users to make arbitrary connections. In the proposed platform, these individual components will write information into a shared file during the compilation process of simulation. A magnetic circuit solver will collect this information and derive the basic matrices and the final companion circuit.

The solver could obtain “from node” number and “to node” number of all magnetic circuit elements. Each node other than the reference node would correspond to a column of incidence matrix $\boldsymbol{A}$. Each magnetic circuit element would be a branch and correspond to a row of matrix $\boldsymbol{A}$. Then for each element, simply write 1 and -1 for “from node” and “to node” to each row of matrix $\boldsymbol{A}$. In this way, without forming equations like (1) and (2), the incidence matrix can be generated. The formation of turns matrix $\boldsymbol{N}$ and permeance matrix $\boldsymbol{P}$ is relatively simple and straightforward.

B. Fixed Matrix UMEC Method

To reduce computation cost in each time step, a fixed matrix solution is desired. To avoid repeating calculations of (15) and (19), the permeance matrix $\boldsymbol{P}$ must be fixed. Thus, instead of using variable reluctance to represent nonlinearity, a fixed reluctance in parallel with a flux source is used as shown in Fig. 4. Either with or without hysteresis, the nonlinear behavior can be properly represented by injecting the flux difference between the actual MMF-Flux curve and linear reluctance curve.

Taking the transformer in Fig. 1 and Fig. 2 as an example. If only branch 5 is modeled with saturation, the magnetic circuit with proposed saturation modeling is shown in Fig. 5.

Equation (1) becomes,

$$\Phi_1 - \Phi_3 - \Phi_5 = \Phi_{sat5} \tag{21}$$

Equation (4) becomes,

$$\boldsymbol{A}^T\boldsymbol{\Phi} = \boldsymbol{\Phi}_{sat} \tag{22}$$

where each element in $\boldsymbol{\Phi}_{sat}$ is the total flux injection from nonlinear reluctances flow into the corresponding node. If multiple nonlinear reluctances are connected to a node, the corresponding element in $\boldsymbol{\Phi}_{sat}$ for this node is the sum up of fluxes injected by all the connected nonlinear reluctances. $\boldsymbol{\Phi}_{sat} = \begin{bmatrix}\Phi_{sa} \\ 0\end{bmatrix}$ in this case.

Apply (22) and (8) to (10).

$$\boldsymbol{\Phi}_{sat} = \boldsymbol{A}^T\boldsymbol{PNi} - \boldsymbol{A}^T\boldsymbol{PA}\,\boldsymbol{\theta}_{node} \tag{23}$$

$$\boldsymbol{\theta}_{node} = (\boldsymbol{A}^T\boldsymbol{PA})^{-1}\boldsymbol{A}^T\boldsymbol{PNi} - (\boldsymbol{A}^T\boldsymbol{PA})^{-1}\boldsymbol{\Phi}_{sat} \tag{24}$$

Left multiplying A,

$$\boldsymbol{\theta} = \boldsymbol{A}(\boldsymbol{A}^T\boldsymbol{PA})^{-1}\boldsymbol{A}^T\boldsymbol{PNi} - \boldsymbol{A}(\boldsymbol{A}^T\boldsymbol{PA})^{-1}\boldsymbol{\Phi}_{sat} \tag{25}$$

Substituting (25) into (9),

$$\boldsymbol{\Phi} = \boldsymbol{MNi} - \boldsymbol{K\Phi}_{sat} \tag{26}$$

where

$$\boldsymbol{K} = \boldsymbol{PA}(\boldsymbol{A}^T\boldsymbol{PA})^{-1} \tag{27}$$

and $\boldsymbol{M}$ remain the same as the classic UMEC in (15).

After partitioning elements not related to windings,

$$\boldsymbol{\Phi}_{ss} = \boldsymbol{M}_{ss}\boldsymbol{N}_{ss}\boldsymbol{i}_{ss} - \boldsymbol{K}_{ss}\boldsymbol{\Phi}_{sat} \tag{28}$$

In this case, $\boldsymbol{K}_{ss} = \begin{bmatrix}K_{11} & K_{12} \\ K_{21} & K_{22}\end{bmatrix}$.

The companion circuit representation can be derived, where conductance matrix is kept same as (19), and historical current source now is,

$$\boldsymbol{i}_{his} = \frac{dt}{2}(\boldsymbol{N}_{ss}\boldsymbol{M}_{ss}\boldsymbol{N}_{ss})^{-1}\boldsymbol{v}(t-dt) + \boldsymbol{i}_{ss}(t-dt)$$
$$+(\boldsymbol{M}_{ss}\boldsymbol{N}_{ss})^{-1}\boldsymbol{K}_{ss}[\boldsymbol{\Phi}_{sat}(t) - \boldsymbol{\Phi}_{sat}(t-dt)] \tag{29}$$

The matrix $\boldsymbol{M}$ and $\boldsymbol{K}$ would remain unchanged throughout the simulation and all the matrices from $\boldsymbol{M}$ to $(\boldsymbol{N}_{ss}\boldsymbol{M}_{ss}\boldsymbol{N}_{ss})^{-1}$ and $(\boldsymbol{M}_{ss}\boldsymbol{N}_{ss})^{-1}\boldsymbol{K}_{ss}$ in (29) can be pre-calculated before the simulation starts. Thus, computation in each time step is minimized and very small time step can be achieved.

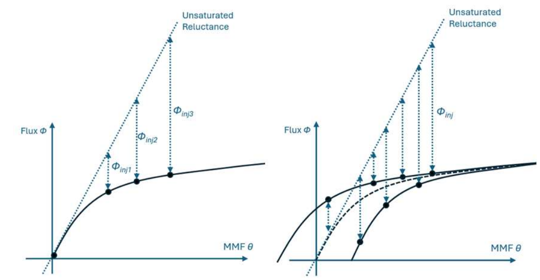

Fig. 4 Injecting flux when saturated while keeping reluctance unchanged, (a) without hysteresis (b) with hysteresis.

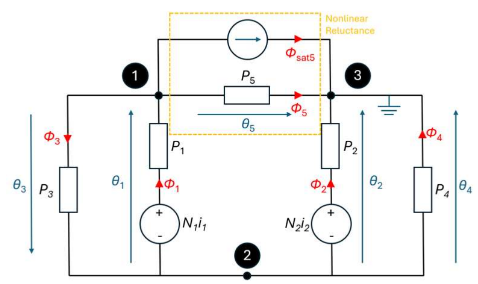

Fig. 5 Equivalent magnetic circuit, nonlinear reluctance on branch 5 is modeled as a linear reluctance in parallel with a flux source.

C. B-H Curve Modeling

The nonlinear reluctances B-H curve, which is equivalent to Flux-MMF curve or Voltage-Magnetizing Current curve, can be represented with different models. For example, the saturation curve can be modeled using linear segments, Langevin function, exponential function or arctangent function [8]; hysteresis can be modeled using Jiles-Atherton or Talukdar methods [9][10]. In this study, arctan representation is used for modeling saturation curve,

$$B = \frac{2B_{sat}}{\pi}\arctan\left(\frac{\pi\mu\mu_0}{2B_{sat}}\cdot H\right) \tag{30}$$

and hysteresis loops are modeled using Talukdar method.

To be noticed, the flux injection is calculated based on the MMFs in the previous time step. This step delay could cause distorted saturation curves, even instability, especially in the deep saturated range where current may change significantly in one time step. The proposed method is designed to be used in very small time step. As a result, delays and the effects can be minimized. Prediction algorithms can be used to predict the MMF, which can further improve the accuracy of saturation curve in simulation. Second order prediction is used in this paper and shows promising results.

IV. Simulation Tests

A. Model Accuracy Benchmark

To demonstrate the model accuracy, a three-phase two-winding three-limb transformer is modeled using proposed approach and is compared to a transformer modeled using RSCAD built-in component - three-phase multi-winding transformer based on Terminal Duality Model (TDM) [11]. The TDM model provides highest fidelity among all the types of transformer models in RSCAD and could use similar saturation/hysteresis modeling approaches as the proposed magnetic circuit simulation tool and thus would provide meaningful benchmarking result.

The test circuits are shown in Fig. 6. The pink color highlights the transformer modeled with magnetic circuit, which consists of windings, linear reluctance representing leakage paths and nonlinear reluctances representing limb and yoke paths. Different from transformers with loose coupled windings in Fig. 1, the realistic transformer windings are arranged as concentric coils [12], and the magnetic circuit is as shown in Fig. 6 (b).

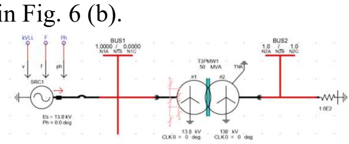

(a)

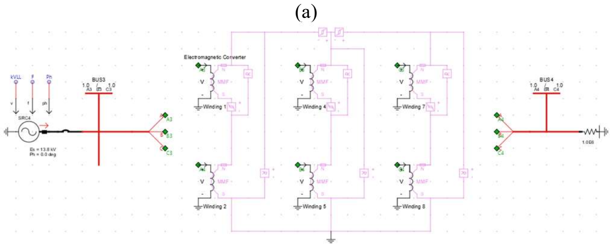

(b)

Fig. 6 Benchmark test circuits, (a) RSCAD TDM transformer model, (b) proposed magnetic circuit model.

Transformer parameters are shown in Table I and magnetic circuit parameters are shown in Table II, where number of winding turns, core material permeability and core section area are selected based on assumptions and all the other magnetic circuit parameters can be calculated from these assumptions and transformer parameters. If the assumptions are made differently, the following parameter calculations will be different, while simulation results, seen from the electric side, will remain the same.

TABLE I Transformer Parameters

Rated Capacity	50 MVA	Knee Voltage	1.263 pu
Base Frequency	60 Hz	Air Core Reactance	0.255 pu
Rated Voltages	13.8/138 kV	Hysteresis Loop Width	10%
Short Circuit Reactance	0.076 pu	Yoke/Limb Length Ratio	1.0413
Magnetizing Current	0.4%	Yoke/Limb Area Ratio	1

TABLE II Magnetic Circuit Parameters

Turns of Winding 1/2	138/1380	Leakage Reluctance	4.96e7 H^{-1}
Core Permeability	4500	Hysteresis Loop Width	54.1A/m
Knee Flux Density	1.81 T	Limb Length/Area	1.33m/0.15m^2
Air Core Permeance	0.036%	Yoke Length/Area	1.38m/0.15m^2

Fig. 7 shows the simulation waveforms of transformer steady state excitation currents and core Flux-MMF curves when the 138 kV side is open (with load resistance of 1e6 Ohm) and the voltage source on the low voltage side is set to 1.1 pu. It can be seen that all the quantities match very well between the two models. The little mismatch is caused by different saturation functions being used that arctan type representation is used for proposed magnetic circuit simulation while quadratic type representation is used in RSCAD TDM transformer models.

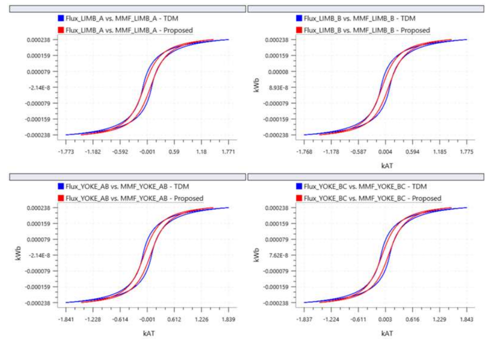

(a)

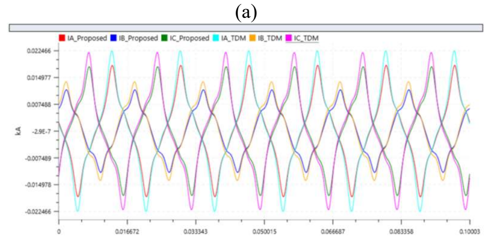

(b)

Fig. 7 Open loop test steady state waveforms, (a) Flux-MMF curves of limbs and yokes, (b) excitation currents.

Fig. 8 shows the simulation waveforms of transformer inrush current test. By opening and then reclosing the breaker in the test circuit, phenomenon of inrush current can be observed, and the inrush current waveforms match well between proposed model and TDM model.

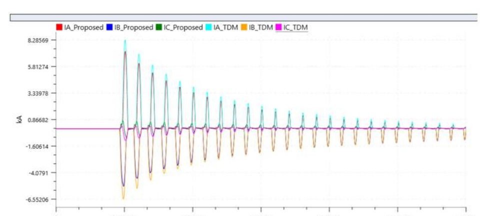

Fig. 8 Benchmark waveforms of inrush current.

B. Computation Cost

The computation cost is benchmarked in terms of required minimum time step for simulating the test circuit as shown in Fig. 6 in real time. Minimum time step means if further reduce time step, computation cannot be completed within one time step. The tests are performed using RTDS NovaCor Light with one core for main circuit and one core for control. The comparison is made among the three models:

1. Proposed magnetic circuit simulation,
2. TDM transformer model,
3. Conventional UMEC transformer model.

The variable matrix methods adopted by TDM and conventional UMEC transformer models are more robust toward the delay in modeling nonlinearity and can be used without problem even with relatively large time steps.

Table III clearly demonstrates the computational efficiency of the proposed method. By leveraging a fixed matrix calculation, the approach significantly reduces the

979-8-3315-8138-1

computational burden in each time step. This enables real-time simulation of complex magnetic circuits with substantially smaller time steps, making it highly suitable for high-frequency and dynamic applications in EMT-type simulators.

Table IV shows the computation cost of proposed model when simulating magnetic circuits of different sizes.

TABLE III MINIMUM TIME STEP FOR TEST CIRCUIT

Proposed	1.9 us
TDM	21 us
Conventional UMEC	14 us

TABLE IV MINIMUM TIME STEP FOR DIFFERENT SIZE OF MAGNETIC CIRCUIT

Circuit in Fig. 6 (b)	1.9 us
Fig. 6 (b) without yoke	1.6 us
Fig.6 (b) with 2 phases only	1.2 us
Fig.6 (b) with 1 phase only	0.8 us

V. APPLICATION EXAMPLE

A specially designed Multi-winding Coupled Inductor (MCI) for achieving zero input current ripple for interleaved DC-DC converter is simulated in this session. Details of the design of this magnetic structure can be found in [13]. The core and winding arrangement of MCI is shown in Fig. 9 (a), the integration of the coupled inductor and power electronic converter is shown in Fig. 9 (b). By properly designing the magnetic circuit, the current ripple on the primary inductors will be transferred to the auxiliary inductors in the form of magnetic energy.

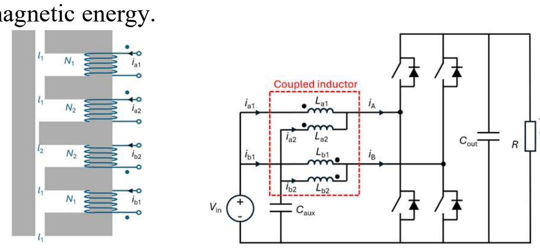

(a) (b)

Fig. 9 Diagrams of zero input current ripple dc-dc converter with MCI, (a) MCI design, (b) converter topology.

Fig. 10 shows the simulation model built in RSCAD. Table V shows the parameters of the simulated circuit. The converter switching frequency is 15 kHz and the whole circuit is simulated with 2 μs time step.

TABLE V CIRCUIT PARAMETERS

Input Voltage Vin	40 V	Auxiliary Capacitance C_{aux}	50 μF
Output Voltage Vout	100 V	Output Capacitance C_{out}	500 μF
Number of Turns N1	20	Number of Turns N2	10
Primary Inductor Self-Inductance La1, Lb1	30 μH	Auxiliary Inductor Self-Inductance La2, Lb2	13.1 μH
Air Gap Ratio l1/l2	4.49	Switching Frequency fsw	15 kHz
Load Resistance Ro	10 Ohm	Simulation Time Step	2 μs

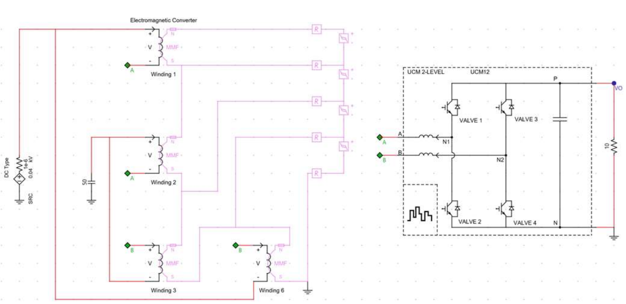

Fig. 10 Simulation circuit of zero input current ripple dc-dc converter.

Fig. 11 shows the simulation results. While the original input currents of the interleaved boost converter i_A and i_B contain heavy harmonic currents, the input currents i_{a1} and i_{b1} have almost zero current ripple that the ripples went through auxiliary inductors and absorbed by the capacitor.

This application example demonstrates that the proposed magnetic circuit modeling approach can effectively simulate arbitrary magnetic core designs, even for high-frequency power electronic applications.

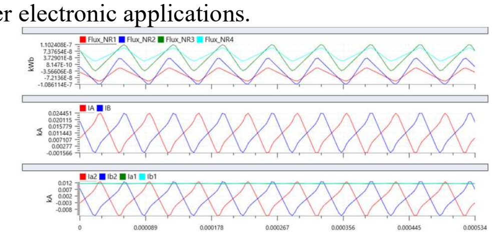

Fig. 11 Simulation waveforms of zero input current ripple dc-dc converter.

VI. CONCLUSIONS

Though the EMT environment inherently is not suitable for simulating multi-domain physics, the proposed method, which is improved from the conventional UMEC algorithm, overcomes the challenge of automating core matrices formation and reducing computation burden. These improvements make it feasible to simulate magnetic circuits with arbitrary topology in real-time EMT environments. Benchmark tests and application examples validate both the flexibility and computational efficiency of the proposed approach, demonstrating its potential for a wide range of power system and power electronics applications.

REFERENCES

[1] T. Zheng, Y. J. Zhao, Y. Jin, P. L. Chen and F. F. Zhang, "Design and Analysis on the Turn-to-Turn Fault Protection Scheme for the Control Winding of a Magnetically Controlled Shunt Reactor," in *IEEE Transactions on Power Delivery*, vol. 30, no. 2, April 2015.

[2] T. Kang, A. Gandomkar, J. Lee and Y. Suh, "Design of Optimized Coupling Factor for Minimum Inductor Current Ripple in DC-DC Converter Using Multiwinding Coupled Inductor," in *IEEE Transactions on Industry Applications*, vol. 57, no. 4, July-Aug. 2021.

[3] H. W. Dommel, *EMTP Theory Book*, 2nd ed. Vancouver, British Columbia, Canada: Microtran Power System Analysis Corporation, 1996.

[4] W. Enright, O.B. Nayak, G.D. Irwin, A. Arrillaga, "An Electromagnetic Transients Model of Multi-Limb Transformer Using Normalized Core Concept", *IPST'97*, Seattle, June 1997, pp.93-98.

[5] W. Enright, N. Waston and O.B. Nayak, "Three Phase five-Limb Unified Magnetic Equivalent Circuit Transformer Models for PSCAD V3", *IPST'99 - International Conference on Power System Transients,* July 20-24, 1999, Budapest, Hungary, pp.462-467.

[6] Y. Zhang, T. Maguire, P. Forsyth, "UMEC Transformer Model for the Real Time Digital Simulator", *IPST 2005*, Montreal Canada, June 2005, Paper No. IPST05-077-25a.

[7] W. Chandrasena, "Development of an improved low frequency transformer model for use in GIC studies," Ph.D. dissertation, Dept. Elect. Comp. Eng., Univ. Manitoba, Winnipeg, Canada, 2003.

[8] R. Szewczyk, "Technical B-H saturation magnetization curve models for SPICE, FEM and MoM simulations," *Journal of Automation, Mobile Robotics & Intelligent Systems*. 10. 3-8.

[9] S. N. Talukdar and J. R. Bailey, "Hysteresis models for system studies," in IEEE Transactions on Power Apparatus and Systems, vol. 95, no. 4, pp. 1429-1434, July 1976.

[10] D. C. Jiles, A. Ramesh, Y. Shi and X. Fang, "Application of the anisotropic extension of the theory of hysteresis to the magnetization curves of crystalline and textured magnetic materials," in IEEE Transactions on Magnetics, vol. 33, no. 5, pp. 3961-3963, Sept. 1997.

[11] M. Ahmadi, A. Dehkordi, Y. Zhang, "Enhancements to Terminal Duality-Based Models for Three-Phase Multi-Limb Multi-Winding Transformers," *IPST 2025,* Guadalajara Mexico, June 2025.

[12] RTDS Technologies Inc., RSCAD User Manual, RTDS Technologies Inc., Winnipeg, Canada, Latest Edition. Available at: https://www.rtds.com/rscad

[13] H. Shen, S. Pan, J. Gong, Q. Hu, Z. Lin and X. Zha, "Design of Magnetic Structure for Zero Input Current Ripple in DC-DC Converter with Multi-winding Coupled Inductor," *2023 IEEE 14th PEDG*, Shanghai, China, 2023, pp. 315-318.